Universal 3D Wearable Fingerprint Targets: Advancing Fingerprint Reader Evaluations

Joshua J. Engelsma, Sunpreet S. Arora, *Member, IEEE,*
Anil K. Jain, *Life Fellow, IEEE,* and Nicholas G. Paulter Jr., *Fellow, IEEE*

***Abstract*—We present the design and manufacturing of high fidelity universal 3D fingerprint targets, which can be imaged on a variety of fingerprint sensing technologies, namely capacitive, contact-optical, and contactless-optical. Universal 3D fingerprint targets enable, for the first time, not only a repeatable and controlled evaluation of fingerprint readers, but also the ability to conduct fingerprint reader interoperability studies. Fingerprint reader interoperability refers to how robust fingerprint recognition systems are to variations in the images acquired by different types of fingerprint readers. To build universal 3D fingerprint targets, we adopt a molding and casting framework consisting of (i) digital mapping of fingerprint images to a negative mold, (ii) CAD modeling a scaffolding system to hold the negative mold, (iii) fabricating the mold and scaffolding system with a high resolution 3D printer, (iv) producing or mixing a material with similar electrical, optical, and mechanical properties to that of the human finger, and (v) fabricating a 3D fingerprint target using controlled casting. Our experiments conducted with PIV and Appendix F certified optical (contact and contactless) and capacitive fingerprint readers demonstrate the usefulness of universal 3D fingerprint targets for controlled and repeatable fingerprint reader evaluations and also fingerprint reader interoperability studies.**

***Index Terms*—3D fingerprint targets, fingerprint reader interoperability, capacitive readers, contact and contactless optical readers**

I. Introduction

AUTOMATED fingerprint identification systems (AFIS) have become increasingly ubiquitous over the last fifty years. With origins in the forensics community in the early 1900s, fingerprints have continued to serve as valuable links to individuals due to their proven uniqueness, permanence, universality, and collectability [1]. More recently, fingerprint recognition systems have exploded into a plethora of niche areas such as mobile device security, healthcare access, financial systems, and government institutions [1]. As fingerprints continue to become a key to access society's confidential data, social benefits, networks, and buildings, the need to know and quantify fingerprint recognition accuracy is paramount. As such, controlled, repeatable evaluations of the various components of fingerprint recognition systems must be performed.

J. J. Engelsma and A. K. Jain are with the Department of Computer Science and Engineering, Michigan State University, East Lansing, MI, 48824
E-mail: {engelsm7, jain}@cse.msu.edu

S. S. Arora was with the Department of Computer Science and Engineering, Michigan State University. He is now with the Risk and Authentication Products organization at Visa Inc., Foster City, CA 94404
Email: sunarora@visa.com

N. G. Paulter Jr. is with the National Institute of Standards and Technology (NIST), Gaithersburg, Maryland 20899
Email: paulter@nist.gov

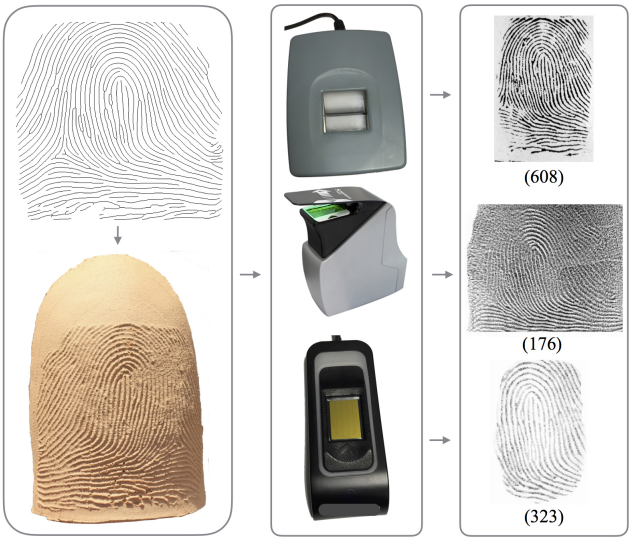

Fig. 1: A Universal 3D Fingerprint Target fabricated in (a) can be imaged by a variety of popular fingerprint readers (contact-optical, contactless-optical, and capacitive) shown in (b). The sensed images of the 3D fingerprint target in (a) are shown in (c). This demonstrates that our targets are appropriate for fingerprint reader interoperability evaluation studies. Similarity scores for each sensed fingerprint image (with the 2D mapped target image) are displayed below each fingerprint image in (c). Verifinger 6.3 SDK was used for generating similarity scores. The score threshold at 0.01 % FAR is 33.

While past end-to-end evaluations such as FpVTE 2012 [2] have provided us with baseline statistics on the performance of state-of-the-art fingerprint recognition systems, much work remains to be done in developing rigorous evaluations of the reader[1] subcomponent of fingerprint recognition systems.

Previous attempts to evaluate the fingerprint reader component have been predominantly undertaken by the FBI and constitute the *Appendix F* and *PIV* standards [18]. The *Appendix F* standard is comparatively stringent, requires pristine image capture, and is designed to facilitate evaluation of fingerprint readers used in person identification scenarios (one to many comparisons). The *PIV* standard is a softer standard than *Appendix F* and is designed to evaluate fingerprint readers used in person verification scenarios (one to one comparison). Both of these standards use imaging targets that are fabricated by projecting a calibration pattern (e.g. sine gratings)

[1]A distinction is made between fingerprint reader and fingerprint sensor. Fingerprint reader refers to the entire device and process, which captures one's physical fingerprint and converts it into a digital image. The sensor is a subcomponent of the reader which converts, through a variety of means (capacitive, frustrated total internal reflection), the physical fingerprint to an electrical signal.

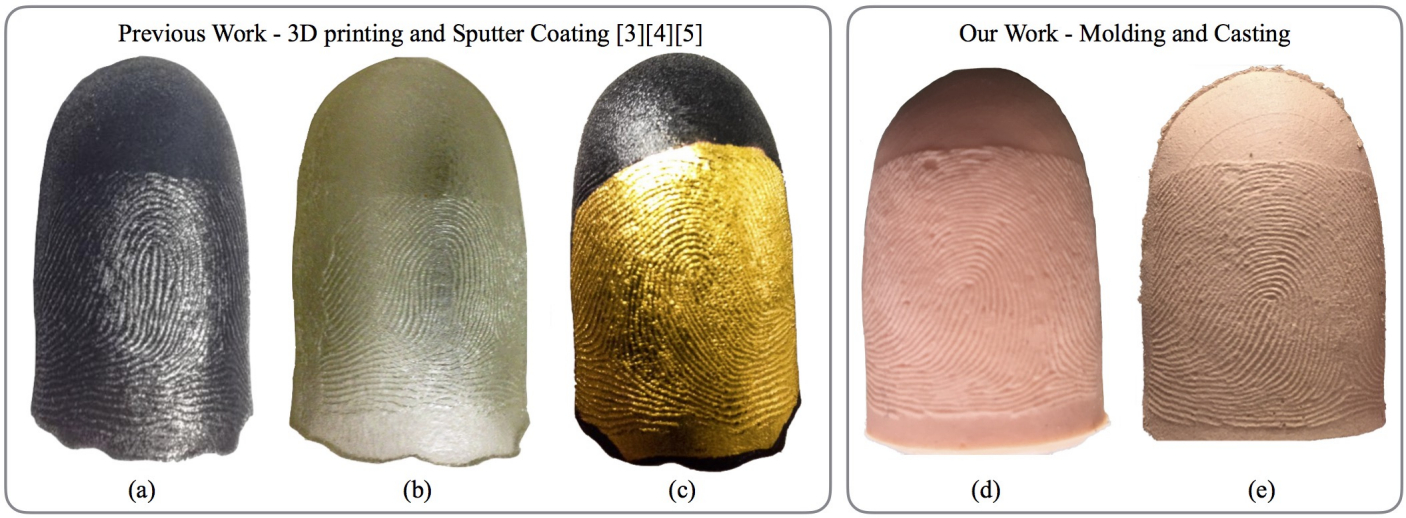

Fig. 2: High fidelity, wearable, 3D fingerprint targets. (a) 3D fingerprint target printed using TangoBlackPlus FLX980 [3], (b) 3D fingerprint target printed using TangoPlus FLX 930 [4], (c) 3D fingerprint target printed using TangoBlackPlus FLX980 and then sputter coated with 30 nm titanium + 300 nm of gold [5], (d) our casted 3D fingerprint target using a mixture of PDMS (Polydimethylsiloxane) and Pantone 488C color pigment [6][7], and (e) our casted universal 3D fingerprint target using a mixture of conductive PDMS, silicone thinner, and Pantone 488C color pigment [6][8][9]. 3D targets in (a), (b), and (c) were printed on a high resolution 3D printer (Stratasys Objet350 Connex).

TABLE I: A Comparison of the Properties of the Human Finger, 3D Printed Targets, and our 3D Casted Targets

Specimen Material	Shore A Hardness	Tensile Strength (MPa)	Elongation at Break (%)	Color	Electrical Resistivity (Ω-cm)	Cost/Target (USD)
Human Skin [10][11][12]	20-41	5-30	35-115	Varies	$2.5 * 10^2 - 8 * 10^6$	N.A.
TangoBlackPlus FLX980 (Fig. 2 (a)) [3][13]	26-28	0.8-1.5	170-220	Black	Insulator	$10.00
TangoPlus FLX930 (Fig. 2 (b)) [4][13]	26-28	0.8-1.5	170-220	Translucent	Insulator	$10.00
TangoBlackPlus FLX980, Ti-Au surface coating (Fig. 2 (c)) [5][13][14]	26-28	0.8-1.5	170-220	Gold	$2.4 * 10^{-5}$	$12.00
PDMS & Pantone 488C Pigment (Fig. 2 (d)) [7]	43	6.7	120	PMS 488C	Insulator	$0.86
Conductive PDMS, Silicone Thinner, & Pantone 488C Pigment (Fig. 2 (e)) [6][8][9]	38.5	2.0	80	Tan / PMS 488C	$9.8 * 10^{-1}$ †	$10.00

† Although the resistivity of the target differs from human skin, the resistivity value is sufficient for image capture by capacitive readers.

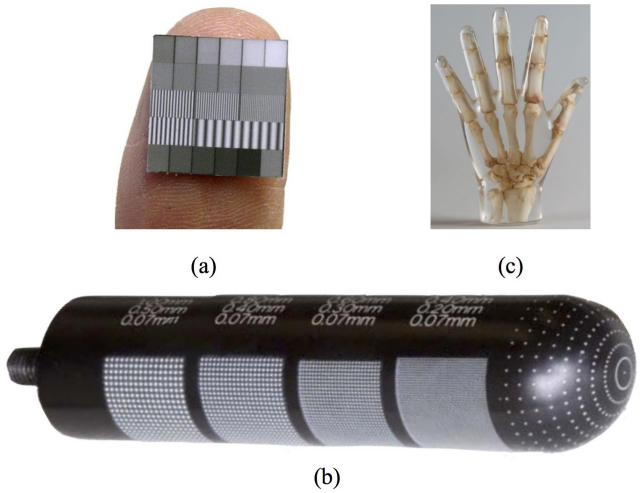

Fig. 3: Examples of Evaluation Targets. (a) standard 2D fingerprint reader calibration target [15]; (b) 3D metal cylinder for contactless fingerprint reader calibration [16]; (c) medical phantom of a human hand [17]. Images taken from [15][16][17]

onto a flat surface (Fig. 3 (a)). These targets are useful for structural (white-box) testing of fingerprint readers since they ensure that certain quantitative imaging thresholds are met by the fingerprint reader's sensing component, however, these targets have little resemblance to the human fingers that the readers will be exposed to in an operational setting. As such, controlled operational (black-box)[2] evaluations of fingerprint readers using the existing standards and targets are limited at best.

To address the challenges of robust operational evaluation inherent to imaging devices, the medical imaging community has developed 3D targets (phantoms) as evaluation specimens. Phantoms are useful for evaluating a variety of medical imaging devices in areas such as radiography, tomography, and ultrasonic imaging [17][20]. Use of live subjects for repeated evaluation of medical devices is impractical because of the health hazards and monetary costs involved. However, realistic 3D phantoms (Fig 3. (c)) make accurate operational evaluation of these devices possible. Proper operational evaluation of fingerprint readers can only be accomplished, in a similar manner, by using 3D fingerprint targets (phantoms) with similar characteristics to the human finger.

[2]White-box testing evaluates the internal sub-components of a system, whereas black-box testing focuses on testing the end-to-end system using system inputs and outputs [19].

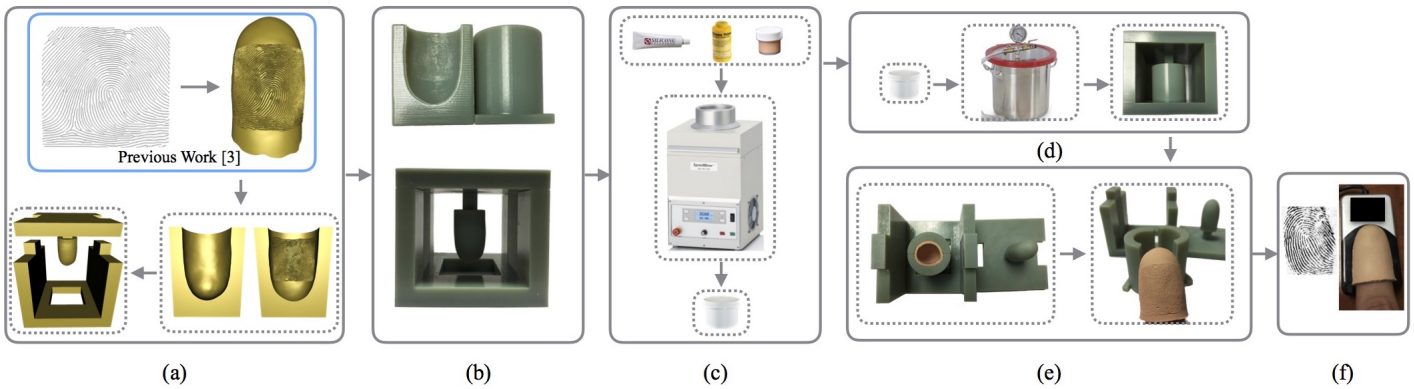

Fig. 4: System block diagram of the proposed molding and casting process for making 3D targets. (a) A 3D negative mold (of a 2D fingerprint image) and a supporting scaffolding system (necessary for making the fingerprint target wearable) are electronically fabricated; (b) 3D electronic models are manufactured by 3D printing and chemical cleaning; (c) conductive silicone, silicone thinner, and human colored dye are mechanically mixed to produce a casting material with similar conductive, mechanical, and optical properties to the human skin; (d) the material fabricated in (c) is cast into the mold and scaffolding system; (d) vacuum degassing ensures that air bubbles are removed from the casted material; (e) wearable fingerprint targets are extracted 72 hours after pouring the casting material; (f) the wearable, 3D fingerprint target is used for fingerprint reader evaluations.

A. 3D Fingerprint Targets

Some research has been conducted developing 3D targets towards achieving the aforementioned goal. In 2011, Orandi et. al developed 3D cylindrical metal targets mapped with 2D calibration patterns for contactless fingerprint readers (Fig. 3 (b)) [21]. However, because these targets are rigid and completely dissimilar in mechanical, optical, and capacitive properties to the human finger, they can not be used by contact-based fingerprint readers. More recently, in 2016, Arora et. al produced high fidelity 3D fingerprint targets using a high resolution, state-of-the-art 3D printer [3][4][5]. These targets were a big step forward in the direction of realistic operational fingerprint reader evaluation because the targets employed a 3D geometry similar to the human finger, they were fabricated using materials with similar mechanical properties as human skin, they were mapped with real fingerprint images, and they could be worn on a human finger. However, due to the limited number of materials that can be used in 3D printers, the polymers used for printing (i) did not have the same nominal electrical conductivity of human skin and (ii) did not have the spectral reflectance of human skin. As a result, multiple types of targets (Figs. 2 (a), (b), (c)) were fabricated for different types of fingerprint readers (capacitive, contact-optical, and contactless-optical) [3][4][5]. These individual targets worked for evaluating the type of reader for which they were designed, however, they were not interoperable. That is, a target fabricated for one type of fingerprint reader (e.g. capacitive) would not work on a different type of fingerprint reader (e.g. optical). Because multiple types of targets were needed for evaluating different types of readers, performing a standardized interoperability evaluation of fingerprint reader technologies was not possible with these 3D printed targets.

B. Fingerprint Reader Interoperability

Past studies on fingerprint reader interoperability have shown that when different fingerprint readers were used for enrollment and identification (or verification), some loss in recognition accuracy ensued [22][23][24]. However, all of these studies were performed on data acquired from live human subjects [25]. As such, variations (finger pressure and orientation; conditions of the finger, e.g. wet or dry) between impressions on the different readers could account for some of the error observed. We posit that in order to truly quantify the effects of interoperability, an interoperable fingerprint target would need to be mounted to a robot gripper and imaged on different readers at the same pressure and orientation.

As noted in [26], continued advances in distributed computing have enabled less monolithic fingerprint recognition systems. This advent of larger, more distributed systems drastically increases the likelihood that the fingerprint reader used to enroll a user's fingerprint image at one location will not be the same reader (or model of reader) used later to identify or verify the same individual at another location. Consider, for instance, India's Aadhaar program, which has already enrolled over 1.14 billion residents (as of May 2017) on a variety of readers, many of whom are receiving services and benefits based on fingerprint and/or iris recognition [27][28]. Furthermore, even if the same reader is used for both enrollment and identification, advances in sensing technology could eventually require replacement of the reader being used. As mentioned in [24], the cost to an institution needing to re-enroll its entire database of users on a new reader could be monumental. Both of these situations underscore the need to know and quantify fingerprint reader interoperability. If fingerprint recognition systems are to continue to become more distributed, then the performance change associated with interoperability must be objectively known and quantified. Doing so will benefit system users, reader manufacturers, system developers, and the institutions deploying the system.

C. Universal 3D Fingerprint Targets

To enable robust, standardized fingerprint reader interoperability evaluations, we present the fabrication of an interoperable 3D fingerprint target (Fig. 1) through a molding and casting process (Fig. 4). We call our target the *universal fingerprint target* (Fig. 2 (e)). Like previous fingerprint targets in [3], the universal fingerprint targets share a 3D geometry similar to a fingerprint surface, have mechanical properties

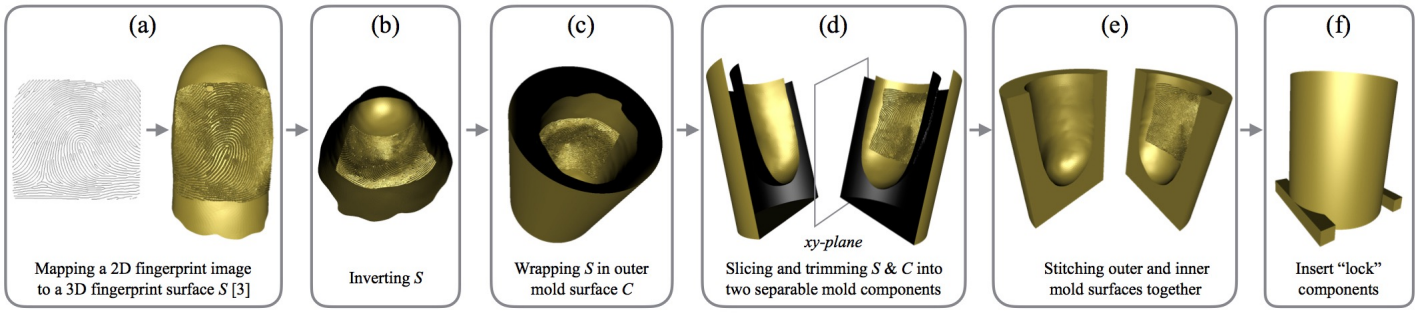

Fig. 5: Process flow for fabricating electronic 3D fingerprint mold, M

similar to human skin, and are mapped with a fingerprint image, either real or synthetic. However, unlike previous fingerprint targets, the universal fingerprint targets are unique in that they incorporate the technically pertinent mechanical, optical, and electrical properties of the human skin within a single target (Table I), making it possible for the universal fingerprint targets to be imaged by all major fingerprint sensing technologies in use (capacitive, contact-optical, contactless-optical)[3]. The universal fingerprint targets enable and facilitate, for the first time, a standardized assessment of fingerprint reader interoperability. The universal fingerprint targets will also enable controlled data collection useful for fingerprint distortion modeling.

More concisely, the contributions of this research are:

- A controlled, repeatable process for creating fingerprint target molds, and fabricating high quality finger castings. Unlike previous works [3], this casting fabrication process is not restricted to a small number of materials. Additionally, it is not cost prohibitive as it is based on a potentially high-throughout casting process.
- Fabricating high fidelity universal 3D fingerprint targets with similar mechanical, optical, and electrical properties to the human skin. Previous targets did not simultaneously possess both the optical and electrical properties of human skin within a single target.
- Fingerprint image capture, using the same 3D target, from optical readers (contact and contactless) and capacitive readers. Our universal fingerprint targets will enable standardized interoperability data collection for the first time ever.
- Experimental evaluations, using the universal 3D fingerprint targets and three different types of commercial off-the-shelf (COTS) fingerprint readers[4] (contact-optical, contactless-optical, and capacitive). Our results quantify the loss in fingerprint recognition accuracy when different readers are used for enrollment and identification (or verification). These findings validate the use of our universal 3D fingerprint target for further fingerprint reader interoperability studies.

[3]We use the term universal to indicate that the targets can be imaged by all existing, major types of fingerprint readers (contact-optical, contactless-optical, and capacitive). Since the submission of this manuscript, we have also verified that the targets can be imaged by Optical Coherence Tomography (OCT), ultrasound, and multispectral fingerprint readers. If new sensing technologies emerge requiring additional properties in casted targets, our flexible casting process allows for concocting a new material with the necessary properties. So, our process can be easily extended to manufacture targets for new fingerprint sensing technologies that may emerge.

[4]Because of our Non-Disclosure Agreement with the vendors, we cannot provide the make and model of the readers used in our experiments.

II. Mold & Scaffold Fabrication

To fabricate a fingerprint target T, we begin by electronically modeling (and subsequently manufacturing) a fingerprint mold M and scaffolding framework F.

A. Mold Fabrication

First, a negative[5] fingerprint mold is electronically designed (Fig. 5), 3D printed, and chemically cleaned. This process is further broken down and expounded upon in the following steps.

i) Inner Mold Surface - Using techniques similar to [3], a 2D fingerprint image is mapped onto a smooth 3D finger surface mesh S in a manner that retains the topology inherent to the 2D image (Fig. 5 (a)). More formally, let S be a mesh of triangular faces $F = \begin{bmatrix} f_1, & f_2, & f_3, & ..., & f_n \end{bmatrix}$, and 3-dimensional vertices $V = \begin{bmatrix} v_1, & v_2, & v_3, & ..., & v_c \end{bmatrix}$. Each face in F is explicitly defined as an ordered list of 3 vertices from V, e.g. $f_1 = \begin{bmatrix} v_i, & v_j, & v_k \end{bmatrix}$. Additionally, every face in F contains a normal vector which is implicitly encoded by the order of the 3 vertices used to define the face. In particular, the direction of the normal vector is determined by taking the cross product of the vectors formed with respect to the order of the face's three vertices. For example, the normal vector for face f_1 is $f_{1,normal} = a \times b$, where a is a vector having tail at v_i and head at v_j, while b is a vector having tail at v_j and head at v_k.

Because the end goal of the electronic modeling of M is to produce a negative mold, the mapped surface S must be inverted by flipping all the faces of S (Fig. 5 (b)). For every face, this flipping is attained by reversing the order of its three vertices - and consequently the implicitly encoded direction of its normal vector. For example, by changing $f_1 = \begin{bmatrix} v_i, & v_j, & v_k \end{bmatrix}$ to $\hat{f}_1 = \begin{bmatrix} v_k, & v_j, & v_i \end{bmatrix}$, the normal vector $\hat{f}_{1,normal}$ computed by $a \times b$ is reversed in direction, since a is now a vector having tail at v_k and head at v_j, while b is a vector having tail at v_j and head at v_i.

ii) Outer Mold Surface - After iteratively inverting all n $\begin{bmatrix} f_1, & f_2, & f_3, & ..., & f_n \end{bmatrix}$ faces, the next step in generating

[5]In molding and casting, positive sculptures are produced from their negative mold.

mold M is to imprint the fingerprint surface S inside of an open ended cylindrical surface C (Fig. 5 (c)). Surface C acts as the exterior of the final mold M. As such, dimensions for C are determined empirically so as to provide strength and durability to the mold and to prevent usage of excess material. Our experiments show that setting the height of C to $C_{height} = 1.25 * S_{height}$ balances the need for structural support and minimizes material cost for casted targets (here S_{height} is the height of the fingerprint surface S). The diameter of the mold (C_{dia}) is fixed at 34 mm. While C_{dia} could have been dynamically chosen based upon the diameter of S (S_{dia}), we chose a fixed value so that all the molds we print could fit within a single scaffolding framework F. We chose 34 mm as a static diameter value, since the 95$^{\text{th}}$ percentile of the widest adult finger (the thumb) is 26 mm to 27 mm [29]. As such, the minimum thickness (t_{min}) of our mold is computed as $t_{min} = 1/2 * (34 - 27)mm = 3.5$ mm. We empirically validated that a mold thickness of $t_{min} \geq 3.5$ mm provides the durability needed for our casting process.

iii) Split Mold - With the inner and outer surface of the mold in place, we continue the fabrication process by simultaneously splitting C and S along the *xy-plane* into C_{above}, S_{above}, C_{below}, and S_{below}. Splitting the mold into two semi-cylindrical components will facilitate the extraction of the final fingerprint castings T (from the mold). C_{above}, S_{above}, C_{below}, and S_{below} are further post processed by adding new faces and vertices such that all four surfaces lie flat on the xy-plane. Figure 5 (d) illustrates the sliced, trimmed, and post processed components C_{below}, C_{above}, S_{below}, and S_{above}.

iv) Stitching and Printing - Finally, the individual surfaces C_{below} and S_{below} and C_{above} and S_{above} are stitched together into two three-dimensional, semi-cylindrical mold halves by adding triangular faces around the periphery of the respective surfaces. Upon completion of this stitching, a high fidelity fingerprint mold M has been electronically fabricated (Fig. 5 (e)).

To minimize the variability of fingerprint targets during consecutive castings, two *"lock"* components are attached to the bottom of C (Fig. 5 (f)). These lock pieces, having length equal to 34 mm (C_{dia}) will prevent C from rotating inside of the scaffolding framework F.

At this point, M is physically realized by using a high resolution, state-of-the-art 3D printer that has the ability to print in slices as small as 16 microns [30]. A printer with such fine resolution is necessary to capture the minute details of the mapped fingerprint onto M[6]. As in [3], the mold is printed in 30 micron layers as this captures the necessary detail of the mapped fingerprints, while simultaneously decreasing the print time of M from 8 hours to 4 hours [3]. At the conclusion of printing, the mold is soaked in 2M NaOH[7] for about 4 hours to dissolve away the support material from the printed mold in a manner that does not damage the fingerprint ridges. After chemical cleaning a high fidelity fingerprint mold is ready for casting fingerprint targets (Fig. 6).

The resultant mold will only produce a solid casting, since casting material will fill the entire mold cavity. To make the cast wearable (e.g. mounting to a robotic gripper) or manual evaluation (e.g. human placement of the target) a *"scaffolding framework"* F is fabricated, which, when used in conjunction with M, creates a wearable 3D target T (Fig. 7). The process for generating F is further expounded upon below.

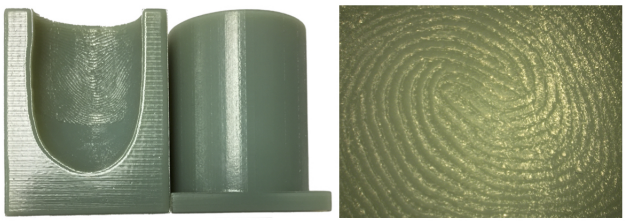

(a) (b)

Fig. 6: (a) High fidelity 3D printed fingerprint mold M. (b) View of fingerprint engraving on M at 20X magnification. The magnified image in (b) shows that all the friction ridge patterns are clearly present in the mold M. These friction ridge patterns are inverted, since negative molds are necessary to produce positive fingerprint targets (Fig 7 (c)).

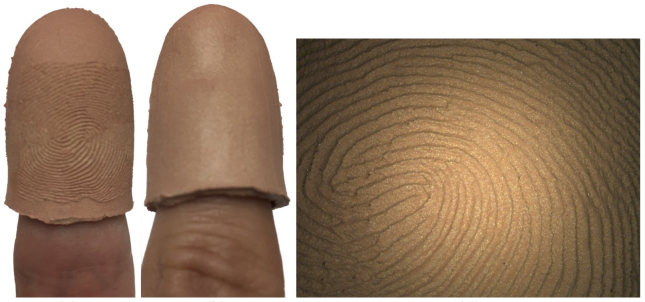

(a) (b) (c)

Fig. 7: 3D wearable Universal Fingerprint Target (a) front view, (b) rear view, and (c) view of the Universal Fingerprint Target ridges at 20X magnification.

B. Scaffolding Fabrication

To create a wearable fingerprint casting, a hollow, appropriately shaped void must be cured into the casted material as it resides in M. This void enables wearability as it creates the space where an end user's finger (or robotic attachment) would reside during evaluation.

We build upon the above idea by developing (based upon the dimensions M) a scaffolding framework F used to insert a fingerprint surface S' (with diameter slightly smaller than S_{dia}) into M during successive fingerprint target casts (Fig. 8 (a)). In doing so, we ensure that when casting material is injected into the mold, the space between S and S' will be filled to form a wearable fingerprint target T.

The scaffolding F consists of several components: a base platform that holds the mold M in place, two sides extending beyond the top of M, and a top piece from which the fingerprint surface S' is suspended. Aside from S', all of these pieces are generated by creating a simple cuboid shape and applying affine transformations until the component is of the correct size and in the correct position. The thickness of scaffolding walls is chosen to be 9 mm, which provides the structural robustness

[6]We also experimented with low resolution printers, however, the resolution was insufficient to cleanly separate the ridges and valleys of a fingerprint pattern.

[7]NaOH (Sodium Hydroxide) is a basic (alkaline) solution that cleans the residual printing support material away from the mold.

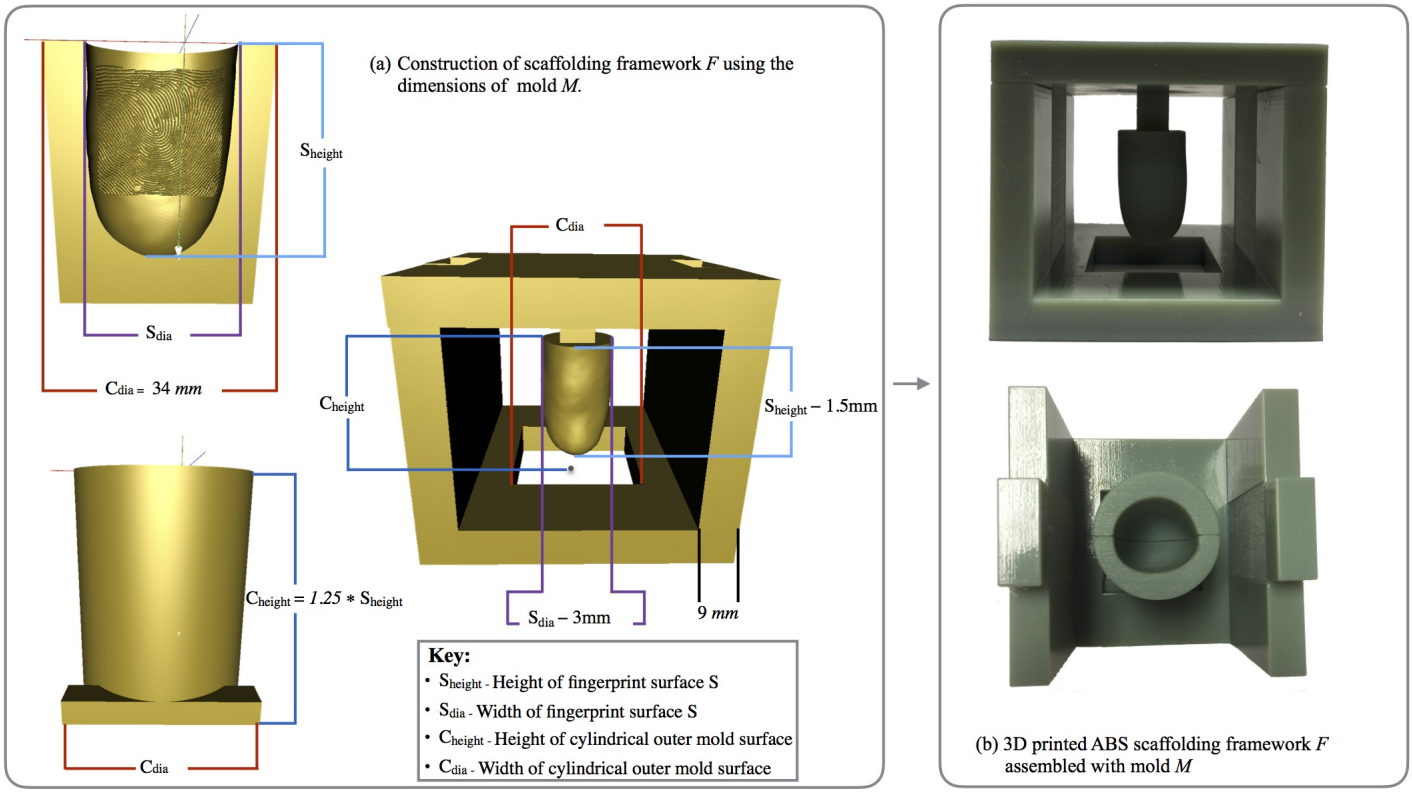

Fig. 8: Fabricating scaffolding F using the dimensions of the mold, M. (a) scaffolding framework F is electronically modeled; (b) the electronic scaffolding system is physically generated in acrylonitrile butadiene styrene (ABS) using a high resolution 3D printer. Using F in conjunction with M, 3D wearable fingerprint targets T are repeatably produced.

and durability needed for repeated castings of fingerprint targets. In addition, a concentric rectangular prism is cut from the inside of the base component. The length and width of this rectangular prism share the same dimension (C_{dia}) as the diameter of M. This ensures that M will attach securely into the base unit, thus controlling the thickness of the casted targets. Since the diameter of M is fixed (based upon the 95th percentile of the human finger width at 34 mm), any mold can be attached interchangeably into a single scaffolding system.

Given that S' is a fingerprint surface with a diameter smaller than S, we can derive S' from the same scanned fingerprint surface that we originally used to generate S. That is, given a smooth scanned 3D fingerprint surface S_{smooth}, we can generate S' by shrinking S_{smooth} along the direction of its normals by 1.5 mm. More formally, if $v_1 = \begin{bmatrix} v_x & v_y & v_z \end{bmatrix}$ is a vertex of S_{smooth} and $n_1 = \begin{bmatrix} n_x & n_y & n_z \end{bmatrix}$ is the corresponding normal vector to v_1, then generating the new vertex $v' = \begin{bmatrix} v'_x & v'_y & v'_z \end{bmatrix}$ for S' is computed as:

$$v' = \begin{bmatrix} v_x \\ v_y \\ v_z \end{bmatrix} - \begin{bmatrix} n_x \\ n_y \\ n_z \end{bmatrix} \times 1.5 \quad (1)$$

After all vertices of S_{smooth} have been iteratively shrunken along the direction of their corresponding normals, the top of S' is stitched shut using a triangle fan[8].

As with M, the electronic model of F is 3D printed using the same high resolution printer and parameters (Fig. 8 (b)). F is also cleaned with 2M NaOH solution to remove residual printing support material. Although F does not have the minute detail that M does, high resolution printing is still needed for printing F so that registration between F and M is consistent and reproducible. This ensures the high fidelity of the casted targets is preserved.

Upon completed fabrication of both M and F, we have tools for repeatably casting high fidelity, 3D wearable fingerprint targets T.

III. Casting

With tools developed for molding and casting in place, we next discuss the characteristics necessary (to emulate human skin) in the casting material for the 3D Universal Fingerprint Target. Additionally, we prescribe a process for concocting a material consisting of these characteristics and subsequently casting the material into a fingerprint mold and scaffolding system.

A. Material Requirements

Our material selection needs to carefully consider the optical, electrical, and mechanical properties inherent to the human finger.

- **Optical Property:** Optical readers rely on proper reflectance and refraction of light rays on the human finger surface to detect a fingerprint. Therefore, the optical properties of the targets must be similar to that of human skin to be accurately sensed by optical readers. Materials

[8]A triangle fan is a circular mesh surface, formed by placing a center vertex and filling in the circle with triangles that all share the center vertex.

that are black will improperly absorb all light rays and materials of high reflectivity will improperly scatter all light rays, in both cases preventing targets of these materials from being imaged by many optical readers.

- **Electrical Property:** In addition to the color attribute, the targets must also be inherently conductive to act as a conductive plate and create capacitive differences between ridges and valleys on the cells within the semiconductor chips on capacitive sensors.
- **Mechanical Property:** Finally, the mechanical properties of the target material must lie within the range inherent to the human epidermis to ensure high quality fingerprint target image acquisition. Materials that deviate from the elasticity of the human epidermis could negatively impact the target in several ways. If the elasticity is too large, the minute details of the minutia will be lost as the target is compressed against the sensor and the ridges collapse under the force being exerted (Fig. 9 (a)). If, on the other hand, the elasticity is too small, or the hardness is too great, the fingerprint target will not flatten around the sensor platen, resulting in only partial print images of the fingerprint surface (Fig. 9 (b)).

(a) 900 % elongation at break (b) Shore A 50

Fig. 9: Fingerprint impressions captured from targets lacking proper mechanical characteristics. Notice (a) the presence of aberrations resulting from excessive elasticity in the target and (b) partial impression due to excessive hardness of the target.

B. Material Fabrication and Casting Procedure

To achieve the electrical, mechanical, and optical criteria necessary for the universal fingerprint target, electrically conductive silicone (SS-27S) [8] is sheer mixed [31] with silicone thinner [9] (at 4 % by mass), and a flesh-toned pigment [6] (at 3 % by mass)[9]. This casting material mixture is transferred to the mold from a disposable pipet. Prior to the transfer, both the mold and scaffolding system are spray coated with silicone release agent [32]. After the material transfer, vacuum degassing at 98 kPa (0.97 atm) removes all air bubbles from the material. Finally, the mold and scaffolding system are assembled and left to cure (Fig. 4 (d)). After 72 hours, a high fidelity, 3D wearable universal fingerprint target, T, can be carefully extracted from the fingerprint mold and scaffolding system (Fig. 4 (e)).

[9]A simpler casting material - useful for interoperability assessment of contact and contactless optical readers - can be fabricated by mixing (with the FlakTek [31]) pure PDMS and PMS 488C pigment. These targets are not conductive, and are therefore unusable for capacitive reader evaluation, but they are optically and mechanically similar to the human finger and are cheaper to manufacture (Fig. 2 (d)) (Table I).

C. Material Characterization

To verify the optical similarity of our fabricated material to human skin, we obtain a spectrogram [33] of the Universal Fingerprint Target material and compare it to a range of human skin spectrograms obtained by NIST [34] from 51 human subjects (Fig. 10). From this spectrogram, it can be seen that the spectral reflectance of the Universal Fingerprint Target material lies within the range of human skin for almost the entire visible spectrum (400 nm - 700 nm). At approximately 625 nm to 700 nm the Universal Fingerprint Target material does deviate from the range of human skin (.05 - .1 reflectance factor). Based on the NIST report, spectral reflectance varies significantly even across multiple readings of the same subject. Furthermore, only 51 subjects were evaluated to establish the range shown in Figure 10. Therefore, it is entirely possible that the Universal Fingerprint Target material does lie within the spectral reflectance of human skin from 625 nm to 700 nm as well, given a larger number of subjects.

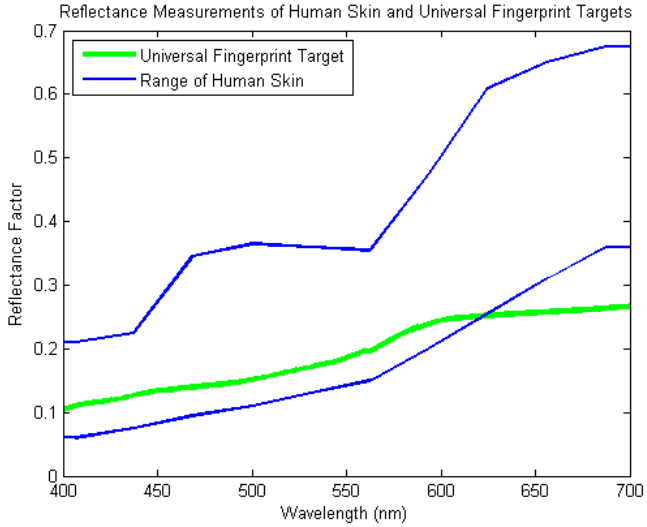

Fig. 10: Comparison of the Universal Fingerprint Target material spectrogram to a range of spectrograms obtained by NIST from 51 human subjects. We plotted the range using estimated data points from the figure in [34].

In addition to verifying optical similarity of the material to human skin, we also verify that the material is electrically conductive by obtaining a resistivity reading (using [36]) from 4 square samples of the material. The average resistivity of the 4 samples is reported in Table I.

Finally, the mechanical properties of the material are computed (using the data-sheets in [8] and [9]) and reported in Table I. From the mechanical values reported in Table I, it can be seen that the chosen material is indeed within the range of the mechanical properties of human skin.

IV. Target Fidelity and Reproducibility

To establish the universal fingerprint targets as standard evaluation artifacts, we must show that the proposed fabrica-

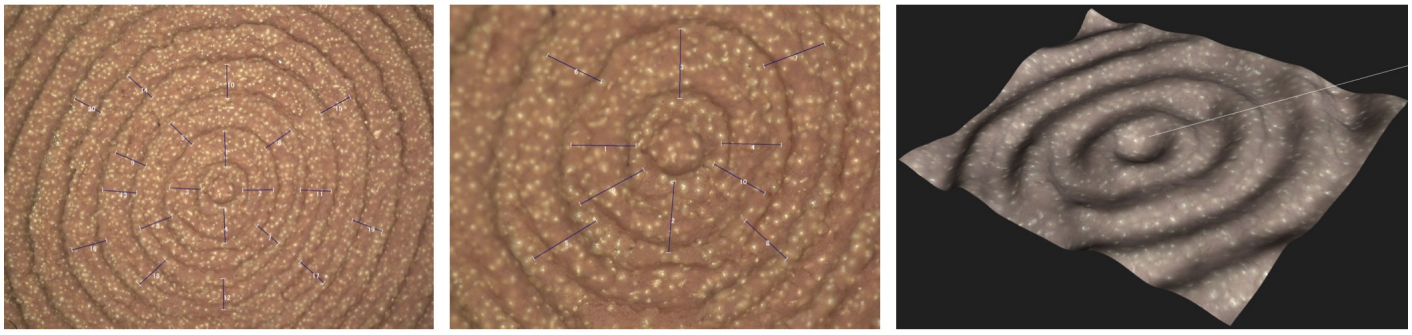

(a) (b) (c)

Fig. 11: Images of the universal fingerprint target (mapped with circular sine gratings) captured using a Keyence optical microscope [35]. Point-to-point ridge distances are measured. (a) Image at 50X magnification and annotated with 20 point-to-point distances. (b) Image at 100X magnification and annotated with 10 point-to-point distances. (c) 3-D image generated by the microscope which qualitatively illustrates the uniformity in ridge height of the circular gratings on the universal fingerprint target. The granular texture in (a), (b), and (c) is evidence of the aluminum coated silver particles mixed into the universal fingerprint target which allows the target to be imaged by capacitive fingerprint readers.

tion process (i) is of high fidelity and (ii) is reproducible. Both of these criterion are verified in the following subsections.

A. Fidelity

A 3D universal fingerprint target is of high fidelity if its 3D ridges retain the topology inherent to the original 2D image it was fabricated from. We posit that fidelity of universal fingerprint targets can be objectively determined and compensated by quantifying the errors (as a deviation of the 3D target topology from the topology of the 2D mapping pattern) at each step in the fabrication process (Fig. 4) and accounting for these errors during fabrication.

(i) Error in Electronic Modeling of Fingerprint Mold - Arora et al. [3] showed that the projection algorithm used to map the 2D fingerprint image to a 3D finger surface results in a 5.8 % decrease in point-to-point distances inherent to the original 2D fingerprint image. Because the electronic fabrication of the fingerprint mold (Fig. 4 (a)) uses the same 2D to 3D projection algorithm as [3], the same error will be encountered in our universal fingerprint target fabrication process.

(ii) Error in 3D printing - Arora et al. [3] also observed an 11.42 % decrease in point-to-point distances (inherent to the original 2D fingerprint image) when fabricating the physical 3D target on a high resolution 3D printer. Since printing the fingerprint mold in (Fig. 4 (b)) was performed using the same printer as [3], the universal fingerprint target fabrication process will encounter the same error.

While the errors introduced in both electronic projection and 3D printing may seem significant, they can be rectified (as shown in [5]) by setting the scale during 2D/3D projection from 19.685 pixels/mm to 16.79 pixels/mm. In doing so, the errors introduced during mold modeling (Fig. 4 (a)) and 3D mold printing (Fig. 4 (b)) are compensated.

(iii) Error in Casting - The fidelity in the universal fingerprint target post casting (Figs. 4 (d), (e)) is validated in the following manner. First, three universal fingerprint target castings are fabricated using three different molds; each mapped with different 2D calibration patterns (vertical, horizontal, and circular sine gratings with a frequency of 10 pixels). At a projection scale of 16.79 pixels/mm (at 500 ppi) and the reduction in point-to-point distances during electronic modeling and 3D printing, 10 pixel ridge distances on the calibration pattern should correspond to an actual ridge distance of 0.508 mm on the casted calibration target. Using an optical microscope, 5 images of each universal fingerprint target are captured at both 50X magnification and 100X magnification (Fig. 11) [35]. A software tool available with the optical microscope is used to mark 20 point-to-point ridge distances at 50X magnification and 10 point-to-point ridge distances at 100X magnification in all the acquired optical microscope images. The microscope software was calibrated using a micrometer resolution calibration target. Table II shows the average point-to-point ridge distances at both magnifications for all 3 casted targets. In comparison to the ground truth distance of 0.508 mm, the optical microscope reveals the empirical mean point-to-point ridge distances to be 0.499 mm, attributing to a 1.8 % reduction in point-to-point distances on the universal fingerprint target during casting. This reduction of 1.8 % in point-to-point ridge distances is not unexpected, since the conductive silicone used to fabricate the universal fingerprint targets is estimated to shrink by 2 % during vulcanization. Again, this error can be compensated by adjusting the projection scale during 2D/3D mapping.

TABLE II: Average point-to-point ridge distances observed on universal fingerprint targets, measured using the Keyence Optical Microscope at 50X and 100X magnification. The expected point-to-point ridge distance is 0.508 mm. (standard deviation is recorded in parenthesis).

Calibration Pattern	50X Magnification	100X Magnification
Vertical Gratings	0.509 mm (.031)	0.496 mm (.023)
Horizontal Gratings	0.501 mm (.026)	0.490 mm (.028)
Circular Gratings	0.513 mm (.029)	0.486 mm (.035)

In addition to measuring point-to-point distances, we also measure the height of the ridges on the casted targets using a high resolution profilometer [37]. The ridge height of the fingerprint targets is set to 0.33 mm during electronic projection. Due to mold shrinkage during 3D printing, we expect the ridge height of the casted targets to be 0.29 mm. The measurements obtained by the profilometer show all ridge heights to be 0.16 mm. This further reduction in ridge height is not unexpected since a thin coating of release agent is first

applied to the mold prior to casting. Furthermore, the reduction in ridge height is beneficial as it brings the ridge height of the targets even closer in value to the human finger ridges at 0.06 mm. Note, the ridge height had to be set to 0.33 mm during electronic projection due to current limitations in state-of-the-art 3D printing resolution. We are currently exploring novel techniques for fabricating the mold which enable even higher resolution than 3D printing.

(iv) End-to-end Error In this final error analysis, the full, end-to-end fabrication process is scrutinized. More specifically, an experiment is conducted which demonstrates that features present on a 2D fingerprint image are preserved after converting the 2D fingerprint image into a wearable, 3D, universal fingerprint target.

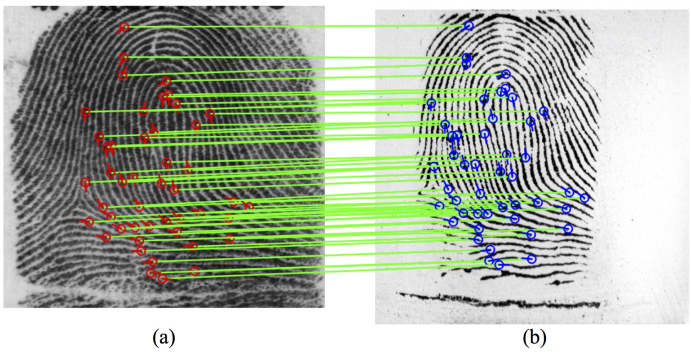

(a) (b)

Fig. 12: Comparing the source fingerprint image to the image of the corresponding universal fingerprint target. (a) NIST SD4 S0083 rolled fingerprint image is compared to (b) a universal fingerprint target image; (b) is fabricated using (a) and imaged using an Appendix F certified, optical, 500 ppi fingerprint reader. A similarity score of 608 is computed between (a) and (b) using Verifinger 6.3 SDK (threshold is 33 at FAR=0.01 %). The minutia points in correspondence between (a) and (b) are shown.

To conduct this experiment, six different universal fingerprint target molds are fabricated using six fingerprint images from the NIST SD4 database [38]. Subsequently, six universal fingerprint targets are cast from the fingerprint molds. Finally, comparison scores are generated between the NIST SD4 rolled fingerprint images and 2D fingerprint images acquired from the corresponding six universal fingerprint targets. Fingerprint images of the universal fingerprint targets are obtained using an Appendix F certified, 500 ppi, contact-optical reader, a PIV certified, 500 ppi, contactless-optical reader, and a PIV certified, 500 ppi, capacitive reader. Figure 12 illustrates corresponding minutia points between a NIST SD4 rolled fingerprint image and a fingerprint image acquired from its corresponding universal fingerprint target. Table III reports similarity scores for each of the six universal fingerprint targets in comparison to the NIST SD4 rolled print used to fabricate them.

The key findings of this experiment are as follows:

- The corresponding minutia points between images captured using the universal fingerprint targets and the images used to generate each target (Fig. 12) show that salient 2D features inherent to the NIST rolled fingerprint images are retained following their fabrication into a universal fingerprint target.
- The universal fingerprint targets (Table III) almost always outperform previous 3D optical targets [3] (Table IV) by achieving higher similarity scores between the finished 3D target images and the ground truth image used to fabricate the respective target. Furthermore, the universal fingerprint targets perform comparably to goldfingers [5] on capacitive readers (Tables III and IV).
- Unlike past research in 3D fingerprint targets, the universal fingerprint target achieves comparison scores on contactless-optical readers well above the acceptance threshold[10] of 33. We do note that the universal fingerprint targets achieve lower comparison scores against the SD4 images when using the contactless-optical reader as opposed to the contact-optical reader for image acquisition. One plausible explanation is that the universal fingerprint targets have a ridge height greater than the ridge height of the adult human finger. This discrepancy may cause errors as the contactless-reader unrolls a 3D fingerprint into a 2D fingerprint image.

TABLE III: Universal Fingerprint Target Similarity Scores[1] (SD4 fingerprint image vs. corresponding target image). Proposed Targets.

SD4 Fingerprint	Contact Optical Reader (500 ppi)	Contactless Optical Reader (500 ppi)	Capacitive Reader (500 ppi)
S0005	584	152	161
S0010	539	137	305
S0031	600	105	221
S0044	498	150	323
S0068	327	146	368
S0083	608	176	323

[1] Verifinger 6.3 SDK was used for generating similarity scores. The score threshold at 0.01 % FAR is 33. Verifinger was chosen so that comparisons could be made between the universal fingerprint targets and previous studies [3][4][5]

TABLE IV: 3D Printed Target[1] Similarity Scores (SD4 fingerprint image vs. corresponding target image). Targets from [3], [5], [4].

SD4 Fingerprint	Contact-Optical Reader (500 ppi) [3], [4]	Capacitive Reader (500 ppi) [5]
S0005	719	471
S0010	129	333
S0031	N/A	N/A
S0044	371	N/A
S0068	N/A	N/A
S0083	441	183

[1] These targets were fabricated using processes reported in [3], [5], [4]. They are not interoperable across optical and capacitive readers as are the Universal Fingerprint Targets.

In summary, the 2D ground truth fingerprint features are found to be preserved during fabrication into a 3D universal fingerprint target and subsequent image acquisition (with high accuracy) by contact-based optical readers, contactless-optical readers, and capacitive readers, as evidenced by the high minutiae-based match scores.

B. Reproducibility

In the previous section, the fabrication process for creating universal fingerprint targets was quantitatively shown to be of high fidelity. One remaining criterion that must be objectively verified to solidify the use of universal fingerprint targets as standardized evaluation artifacts is the reproducibility of high

[10]We use Verifinger 6.3 which has a threshold of 33 at a FAR=0.01%.

TABLE V: Universal Fingerprint Target Genuine Similarity Scores[1] (SD4 Fingerprint Image vs. Corresponding Target Image) Mean and (Standard Deviation) of Scores for 10 Impressions are Reported

Target Set	Reader	S0005	S0010	S0031	S0044	S0068	S0083
T_1	Contact-Optical (*COR_A*)	212.2 (19.97)	200.3 (15.76)	204.4 (19.28)	177.0 (23.13)	141.3 (8.99)	254.5 (20.09)
T_2	Contact-Optical (*COR_A*)	247.4 (10.32)	207.0 (9.17)	226.8 (17.31)	230.6 (16.04)	166.5 (10.01)	248.7 (8.44)
T_1	Contactless-Optical (*CLOR*)	203.9 (15.75)	127.5 (15.22)	140.6 (7.83)	154.3 (11.76)	169.9 (17.29)	172.8 (17.81)
T_2	Contactless-Optical (*CLOR*)	205.1 (14.09)	134.3 (23.01)	150.7 (10.28)	143.4 (15.73)	170.5 (22.16)	172.0 (11.51)
T_1	Capacitive (*CPR_A*)	163.2 (21.81)	128.6 (25.22)	177.1 (14.47)	141.3 (22.74)	121.3 (14.20)	190.9 (17.14)
T_2	Capacitive (*CPR_A*)	188.1 (16.68)	183.8 (16.50)	194.4 (21.63)	173.3 (10.42)	156.5 (6.95)	194.0 (6.65)

[1] Innovatrics matcher was used to generate similarity scores. The threshold of the matcher at FAR = 0.01 % was computed to be 49 on the FVC 2002 and 2004 databases [39], [40].

TABLE VI: Specifications of the Fingerprint Readers Used in Our Experiments

Reader NDA Alias[1]	Reader Type	Resolution	Certifications
COR_A	Contact-Optical	500 *ppi*	Appendix F
COR_B	Contact-Optical	500 *ppi*	Appendix F
$CLOR$	Contactless-Optical	500 *ppi*	PIV
CPR_A	Capacitive	500 *ppi*	PIV
CPR_B	Capacitive	500 *ppi*	PIV

[1] Because of a Nondisclosure agreement (NDA) with our vendors, we do not release the names of the fingerprint readers.

fidelity universal fingerprint target fabrication. To that end, we individually examine the reproducibility of each step in the universal fingerprint target fabrication process.

The electronic model of the universal fingerprint target mold and scaffolding system can be easily reproduced by simply executing a program. Additionally, the mold and scaffolding system can be physically reproduced via 3D printing with accuracy as high as 20 microns [30]. Therefore, the only step in the universal fingerprint target fabrication process that must still be verified as reproducible is the casting step.

To demonstrate reproducibility in casting, 12 universal fingerprint targets are fabricated from 6 fingerprint molds. The 12 universal fingerprint targets correspond to 6 different targets each fabricated 2 times (with a time lapse of several weeks between target replication). Each mold is mapped with one of 6 NIST SD4 rolled fingerprint images (S0005, S0010, S0031, S0044, S0068, and S0083). Let the two sets of universal fingerprint targets be formally defined as T_1 and T_2, where T_1 is the first set of castings and T_2 is the set of castings produced several weeks later.

Next, the average and standard deviation of genuine scores between 10 impressions from each target in the two target sets T_1 and T_2 collected on 3 types of fingerprint readers (*COR_A*, *CLOR*, and *CPR_A* (Table VI)) and the corresponding fingerprint image in NIST SD4 are computed using the Innovatrics fingerprint SDK[11] [41]. The averages and standard deviations of genuine similarity scores between target impressions from each target in T_1 and its corresponding fingerprint image in NIST SD4 are formally defined as GS_1. Conversely, GS_2 is defined as the averages and standard deviations of genuine similarity scores between target impressions for each target in T_2 and its corresponding fingerprint image in NIST SD4.

[11]We use the Innovatrics fingerprint SDK since we recently acquired this matcher, and it is shown to have high accuracy. Mention of any products or manufacturers does not imply endorsement by the authors or their institutions of these products or their manufacturers.

By analyzing the means of the similarity scores in GS_1 and GS_2, reproducibility in casting universal fingerprint targets is verified. In particular, by showing that the means of the similarity scores in GS_1 and GS_2 are all well above the genuine acceptance threshold, we demonstrate that targets (from multiple castings) in T_1 and T_2 are all of high fidelity, since impressions from both sets of targets (on multiple types of fingerprint readers) achieve high similarity scores against the ground truth images (SD4) from which they were fabricated. The means and standard deviations of the genuine similarity scores in GS_1 and GS_2 are reported in Table V.

We note that the means of all similarity scores in GS_1 and GS_2 are within 0.72 % when using the contactless fingerprint reader for image acquisition (Table V). This indicates high similarity between 3D fingerprint topologies on targets in T_1 and T_2. Additionally we note that the means of similarity scores in GS_1 and GS_2 differ slightly when using contact based fingerprint readers for image acquisition. This is not surprising since the targets in T_1 were fabricated with smaller amounts of silicone thinner than the targets in T_2. As such, the softer targets in T_2 morphed around the fingerprint reader platen more than the targets in T_1 and produced images with larger friction ridge area and number of minutia (recall Fig. 9 (b)). Subsequently, the larger fingerprint images acquired from targets in T_2 achieved higher match scores against SD4 images than fingerprint images acquired from targets in T_1. This finding underscores one of the key advantages of contactless fingerprint readers. In particular, it shows that contactless readers are robust to small mechanical variations in human finger epidermis.

V. Experiments

With the fidelity and reproducibility of the universal fingerprint target fabrication process established, multiple experiments are performed on all three major types of fingerprint readers using universal fingerprint targets as operational evaluation targets. First, three fingerprint readers (*COR_A, CLOR*, and *CPR_A* (Table VI)) are individually assessed using three different universal fingerprint targets mapped with controlled calibration patterns (horizontal gratings, vertical gratings, and circular gratings). Next, the same three fingerprint readers are individually evaluated using impressions acquired from fingerprint targets in T_2. Finally, a fingerprint reader interoperability study is performed by comparing images acquired from one of three reader types (contact-optical, contactless-optical, and capacitive) against images acquired from another of the three reader types.

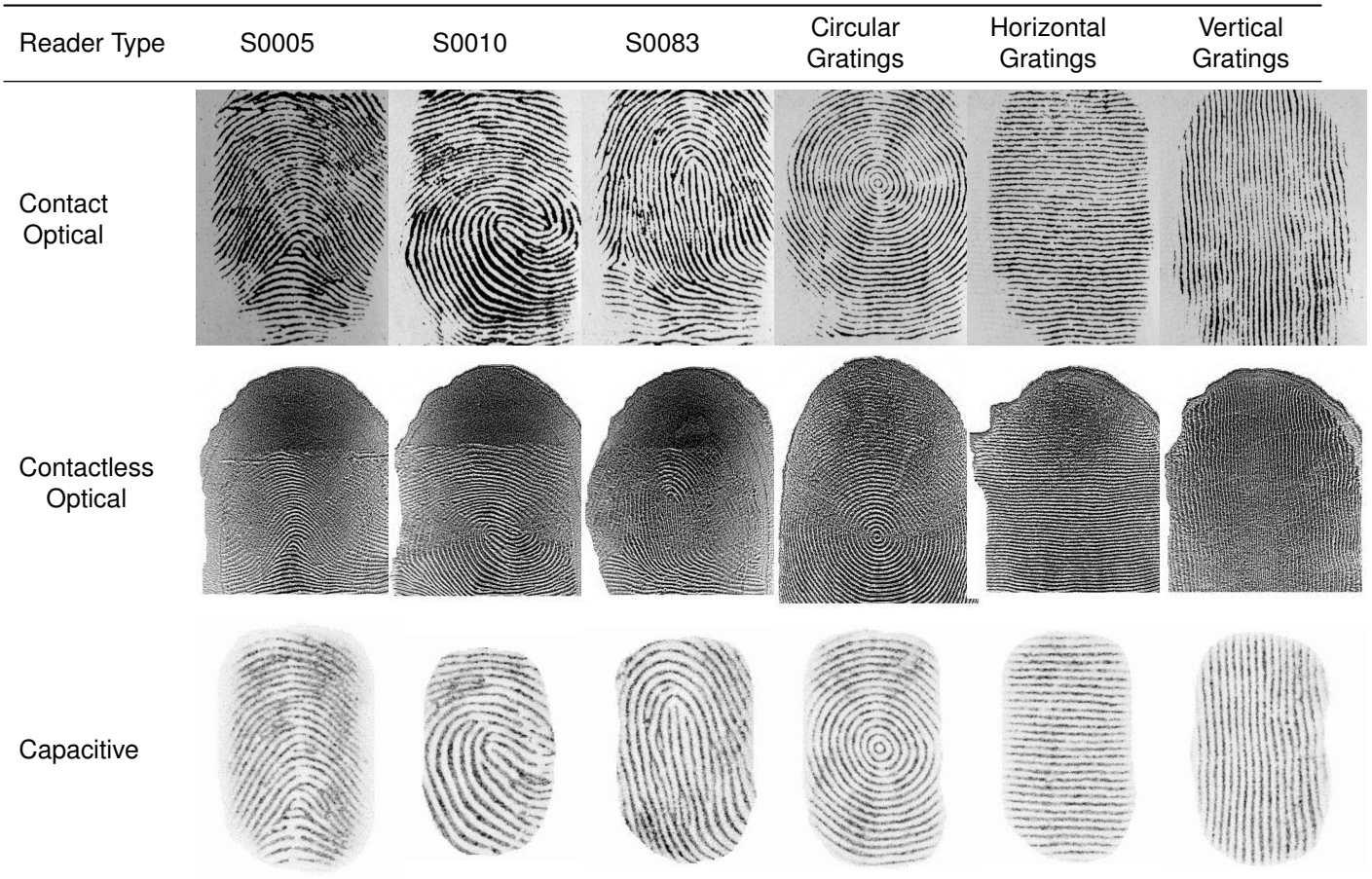

Fig. 13: Example fingerprint impressions from 6 universal fingerprint targets (one per column) on 3 types of fingerprint readers.

TABLE VII: Mean (μ) and std. deviation (σ) of center-to-center ridge spacings (in pixels) on images acquired from 3 universal fingerprint targets. The expected ridge spacing is 9.8 pixels[1].

Sine Gratings Pattern	Contact Optical (*COR_A*)	Contactless Optical (*CLOR*)	Capacitive (*CPR_A*)
Circular	$\mu = 9.50$ $\sigma = 0.56$	$\mu = 8.99$ $\sigma = 0.06$	$\mu = 9.75$ $\sigma = 0.12$
Horizontal	$\mu = 9.21$ $\sigma = 0.65$	$\mu = 8.94$ $\sigma = 0.16$	$\mu = 9.45$ $\sigma = 0.10$
Vertical	$\mu = 8.90$ $\sigma = 0.88$	$\mu = 7.63$ $\sigma = 0.51$	$\mu = 9.17$ $\sigma = 0.09$

[1] Refer to section V,A for expected ridge spacing calculation.

TABLE VIII: Mean (μ) and std. deviation (σ) of center-to-center ridge spacings (in pixels) on images acquired from 3D printed targets[1]. The expected ridge spacing is 8.28 pixels.

Sine Gratings Pattern	Contact Optical [3]	Contactless Optical [4]	Capacitive[2] [5]
Circular	$\mu = 8.92$ $\sigma = 0.04$	$\mu = 8.12$ $\sigma = 0.16$	N/A
Horizontal	$\mu = 8.31$ $\sigma = 0.10$	N/A	N/A
Vertical	$\mu = 8.87$ $\sigma = 0.08$	N/A	N/A

[1] These targets were fabricated using processes reported in [3], [4], [5]. They are not interoperable across optical and capacitive readers as are the Universal Fingerprint Targets.
[2] No ridge spacing results were reported for sine grating mapped gold fingers in [5].

A. Evaluating Readers with Calibration Patterns

To evaluate the directional imaging capability of fingerprint readers, we design a similar experiment to that which is proposed in [3]. In particular, we collect 10 impressions on 3 different types of fingerprint readers using 3 different universal fingerprint targets mapped with controlled calibration patterns (example impressions shown in Fig. 13). Then, using the method in [42] the average ridge-to-ridge spacing (in pixels) is computed for the captured impressions. Unlike the targets proposed in [3], [4], [5] which could only perform directional assessment of one type of fingerprint reader, our proposed universal fingerprint targets are capable of performing directional assessment on contact-optical, contactless-optical, and capacitive fingerprint readers alike. Therefore, in Table VII, we report the average ridge-to-ridge spacing of the 3 different universal fingerprint targets across all three of the major fingerprint reader types. For comparison to previous work [3], [4], [5], the ridge spacing values acquired from sine grating mapped, 3D printed targets (using several fabrication processes) are reported in Table VIII.

All three of the calibration patterns that were mapped to universal fingerprint targets have a 10 pixel peak-to-peak frequency. Given our earlier findings of an approximately 2 % decrease in point-to-point distances on the universal fin-

gerprint targets during fabrication (due to silicone shrinkage), ridge-to-ridge distances on the 3 calibration mapped universal fingerprint targets are expected to be 9.8 pixels. Given this ground truth value and the results of Table VII, we can evaluate the three types of fingerprint readers used in this experiment.

The summary of our findings are as follows:

- Similar to the findings of [3], impressions of targets mapped with circular gratings have larger ridge-to-ridge spacing than impressions of targets mapped with horizontal or vertical gratings. As noted in [3], this is likely due to the radial flattening of the target with circular gratings as it is applied with pressure to the fingerprint reader platen. This radial flattening results in larger ridge-to-ridge spacing than the flattening of the horizontal and vertical calibration targets.
- Unlike the findings of [3], all of the captured impressions of universal fingerprint targets have smaller ridge-to-ridge spacing than the expected ridge-to-ridge spacing. In [3] a larger than expected ridge-to-ridge spacing was explained as a result of ridge-to-ridge distance expansion during the flattening of the target against the reader platen. We hypothesize that universal fingerprint targets have smaller ridge-to-ridge expansion during contact with the reader platen than [3] since universal fingerprint targets are less elastic than the targets in [3]. Universal fingerprint targets are closer in elasticity to the human skin than [3] and so the results shown in Table VII are more indicative of the ridge-to-ridge spacing the readers used in this study are able to capture from real human fingers.
- Consistent with the findings of [4], the ridge-to-ridge distances are smaller on the contactless fingerprint reader than on the contact fingerprint readers. In particular, the captured ridge-to-ridge spacing of the vertical gratings was lower than expected. We hypothesize that the ridge-to-ridge spacing on the contactless reader is smaller due to the fact that no distortion occurs during image acquisition (as no pressure is applied onto a reader platen). Further analysis needs to be undertaken to understand why the vertical gratings deviated most from the expected ridge spacing.

B. Evaluating Readers with Fingerprint Patterns

Similar to the previous experiment, we conduct an analysis of the ridge-to-ridge distances captured by three of the major fingerprint reader types. However, in this experiment, rather than mapping controlled calibration patterns to universal fingerprint targets, we use the targets from T_2 which are each mapped with real fingerprint images from SD4. In doing so, we evaluate the readers with targets very similar to the real fingers the readers will see in an operational setting.

Again, 10 impressions are captured on all 3 fingerprint readers, this time with each of the 6 universal fingerprint targets in T_2 (example impressions shown in Fig. 13). Then, using the method in [42], the average ridge spacing of the captured impressions is computed (Table IX). Additionally, the average ridge spacing is computed (using the method in [42]) on the original fingerprint images from SD4 and established as the ground truth ridge spacing values. By comparing these ground truth values with the results of Table IX, we perform an assessment of the three fingerprint readers. Finally, for comparison to previous work [3], [4], [5], the ridge spacing values acquired from fingerprint mapped, 3D printed targets (using several fabrication processes) are reported in Table X.

TABLE IX: Mean (μ) and std. deviation (σ) of center-to-center ridge spacings (in pixels) on images acquired from 6 universal fingerprint targets. Expected ridge spacing (in pixels) for each target is reported in parenthesis

SD4 Fingerprint	Contact Optical (*COR_A*)	Contactless Optical (*CLOR*)	Capacitive (*CPR_A*)
S0005 (9.25)	$\mu = 8.77$ $\sigma = 1.17$	$\mu = 8.77$ $\sigma = 0.31$	$\mu = 9.01$ $\sigma = 0.18$
S0010 (9.98)	$\mu = 9.87$ $\sigma = 1.46$	$\mu = 9.52$ $\sigma = 0.29$	$\mu = 10.42$ $\sigma = 0.41$
S0031 (10.37)	$\mu = 10.02$ $\sigma = 1.40$	$\mu = 9.04$ $\sigma = 0.37$	$\mu = 10.45$ $\sigma = 0.28$
S0044 (9.07)	$\mu = 8.49$ $\sigma = 1.24$	$\mu = 8.25$ $\sigma = 0.18$	$\mu = 9.04$ $\sigma = 0.23$
S0068 (9.48)	$\mu = 9.60$ $\sigma = 1.29$	$\mu = 9.18$ $\sigma = 0.29$	$\mu = 9.86$ $\sigma = 0.19$
S0083 (10.23)	$\mu = 9.70$ $\sigma = 1.23$	$\mu = 8.16$ $\sigma = 0.15$	$\mu = 10.23$ $\sigma = 0.14$

TABLE X: Mean (μ) and std. deviation (σ) of center-to-center ridge spacings (in pixels) on images acquired from 3D printed fingerprint targets[1]. Expected ridge spacing (in pixels) for each target is reported in parenthesis

SD4 Fingerprint	Contact Optical [3]	Contactless Optical[2] [4]	Capacitive [5]
S0005	$\mu = 8.49$ $\sigma = 0.10$ (7.82)	N/A	$\mu = 9.57$ $\sigma = 0.14$ (9.45)
S0010	$\mu = 9.22$ $\sigma = 0.16$ (8.43)	N/A	$\mu = 10.34$ $\sigma = 0.21$ (10.20)
S0083	$\mu = 9.10$ $\sigma = 0.19$ (8.62)	N/A	$\mu = 10.60$ $\sigma = 0.14$ (10.44)

[1] These targets were fabricated using different processes reported in [3], [4], [5]. They are not interoperable across optical and capacitive readers as are the Universal Fingerprint Targets.
[2] No ridge spacing results were reported for fingerprint mapped targets imaged by a contactless reader in [4].

In summary, the findings of this experiment are as follows:

- Consistent with the findings of our previous experiment with calibration pattern mapped universal fingerprint targets, the images captured by the contactless-optical fingerprint reader have smaller ridge-to-ridge distances than the impressions captured by contact based readers. This is likely due to the absence of fingerprint distortions in contactless fingerprint readers. Additionally, errors in the contactless reader may be introduced when the three-dimensional finger surface captured by the reader is projected into two dimensions (due to the ridge height of universal fingerprint targets being greater than the ridge height of human fingers).
- In almost all of the target impressions, capacitive fingerprint readers captured the ridge-to-ridge distances more closely to ground truth than contact-optical readers did. Further studies and analysis need to be performed to

TABLE XI: Genuine and Imposter Score[1] Statistics and Matching Performance Measures when Comparing Fingerprint Images Acquired from Different Types of Fingerprint Readers. Mean of Genuine Scores (μG), Mean of Imposter Scores (μI), True Accept Rate (TAR) and False Accept Rate (FAR) are Reported.

	Probe Image Fingerprint Readers				
Enrollment Image Fingerprint Readers	Contact-Optical *COR_A*	Contact-Optical *COR_B*	Contactless-Optical *CLOR*	Capacitive *CPR_A*	Capacitive *CPR_B*
Contact-Optical *COR_A*	$\mu G = 440.69$, $\mu I = 0.46$ $TAR = 100\%$, $FAR = 0.0\%$	$\mu G = 399.63$, $\mu I = 0.33$ $TAR = 100\%$, $FAR = 0.0\%$	$\mu G = 182.20$, $\mu I = 1.16$ $TAR = 100\%$, $FAR = 0.0\%$	$\mu G = 275.99$, $\mu I = 1.88$ $TAR = 100\%$, $FAR = 0.0\%$	$\mu G = 202.43$, $\mu I = 4.76$ $TAR = 100\%$, $FAR = 0.0\%$
Contact-Optical *COR_B*	$\mu G = 399.32$, $\mu I = 0.28$ $TAR = 100\%$, $FAR = 0.0\%$	$\mu G = 438.06$, $\mu I = 0.17$ $TAR = 100\%$, $FAR = 0.0\%$	$\mu G = 171.30$, $\mu I = 0.50$ $TAR = 99.83\%$, $FAR = 0.0\%$	$\mu G = 278.54$, $\mu I = 1.57$ $TAR = 100\%$, $FAR = 0.0\%$	$\mu G = 200.03$, $\mu I = 4.25$ $TAR = 100\%$, $FAR = 0.0\%$
Contactless-Optical *CLOR*	$\mu G = 183.76$, $\mu I = 1.39$ $TAR = 100\%$, $FAR = 0.0\%$	$\mu G = 174.29$, $\mu I = 0.54$ $TAR = 100\%$, $FAR = 0.0\%$	$\mu G = 334.06$, $\mu I = 8.99$ $TAR = 100\%$, $FAR = 0.0\%$	$\mu G = 154.06$, $\mu I = 2.11$ $TAR = 99.83\%$, $FAR = 0.0\%$	$\mu G = 113.20$, $\mu I = 4.59$ $TAR = 94.83\%$, $FAR = 0.0\%$
Capacitive *CPR_A*	$\mu G = 271.07$, $\mu I = 0.83$ $TAR = 100\%$, $FAR = 0.0\%$	$\mu G = 274.71$, $\mu I = 0.83$ $TAR = 100\%$, $FAR = 0.0\%$	$\mu G = 146.99$, $\mu I = 1.63$ $TAR = 99.67\%$, $FAR = 0.0\%$	$\mu G = 352.99$, $\mu I = 7.58$ $TAR = 100\%$, $FAR = 0.0\%$	$\mu G = 269.37$, $\mu I = 12.08$ $TAR = 100\%$, $FAR = 0.0\%$
Capacitive *CPR_B*	$\mu G = 196.40$, $\mu I = 2.26$ $TAR = 100\%$, $FAR = 0.0\%$	$\mu G = 195.38$, $\mu I = 2.24$ $TAR = 100\%$, $FAR = 0.0\%$	$\mu G = 105.37$, $\mu I = 3.237$ $TAR = 91.83\%$, $FAR = 0.0\%$	$\mu G = 268.16$, $\mu I = 10.08$ $TAR = 100\%$, $FAR = 0.0\%$	$\mu G = 277.48$, $\mu I = 14.35$ $TAR = 100\%$, $FAR = 0.0\%$

[1] Innovatrics matcher was used to generate similarity scores. The threshold of the matcher at FAR = 0.01 % was computed to be 49 on the FVC 2002 and 2004 databases [39], [40].

determine if this finding is consistent, and also, the explanation behind this.

C. Reader Interoperability Evaluations

Whereas our previous two experiments with universal fingerprint targets evaluated the three major types of fingerprint readers individually, in this final experiment, we perform fingerprint reader *interoperability* evaluations using the universal fingerprint targets.

To set up this experiment, 10 impressions from each target in T_2 are captured on 5 different fingerprint readers (Table VI). Then, for all pairs of fingerprint readers in our set of 5 readers, images from one reader are used as enrollment images and images from the other reader are used as probe images to generate genuine and imposter scores using the Innovatrics matcher [41]. In Table XI, we report the means of the genuine and imposter scores. Additionally we report the True Accept Rate (TAR) and the False Accept Rate (FAR) of the scores using a threshold of 49 (this threshold was precomputed on the FVC 2002 and 2004 databases [39], [40], because we do not have a sufficient number of images from the targets to set the threshold).

Although the performance results of Table XI seem to indicate that all of the readers used are highly interoperable, these results are likely too optimistic as only 6 different targets were used. For this reason, we also report the genuine and imposter score means to show how the scores deteriorate when different readers are used for enrollment and verification. Similar to the findings of past fingerprint reader interoperability studies [22], [23], [24], we note that genuine scores decrease and imposter scores increase when different fingerprint readers are used to acquire enrollment images and probe images, especially when the two readers use different sensing technology to acquire images. While past studies reported these findings using real fingers for data collection, we report the same findings, for the first time ever, using realistic, 3D, wearable, fingerprint targets. By demonstrating the same results as past studies with the universal fingerprint targets, we validate the utility in using universal fingerprint targets for advancing fingerprint reader interoperability studies. In particular, the universal fingerprint targets could be mounted to a robot and imaged on different readers at known pressure and orientation. This standardized data could then be used to learn calibration mappings between different fingerprint readers which could be used to improve fingerprint reader interoperability.

VI. Conclusions and Future Work

We have designed a molding and casting system capable of fabricating wearable, 3D fingerprint targets from a plethora of casting materials. By selecting a casting material with similar mechanical, optical, and electrical properties to the human skin, we cast *universal fingerprint targets*, which can be imaged on the three major fingerprint reader types in use (contact-optical, contactless-optical, and capacitive). Previous studies were unable to produce a single 3D fingerprint target which could be imaged on multiple types of fingerprint readers. We demonstrate that the process for fabricating universal fingerprint targets is of high fidelity, and that it is reproducible. Finally, we use the universal fingerprint targets as evaluation targets on multiple types of PIV/Appendix F certified fingerprint readers. Our results verify the utility in using the universal fingerprint targets for both individual fingerprint reader assessments and also fingerprint reader interoperability studies. We believe that the universal 3D fingerprint targets introduced here will advance state of the art in fingerprint reader evaluation and interoperability studies.

In the future, the universal fingerprint targets will be mounted to a robotic hand and imaged on various fingerprint readers at known pressure and orientation. With this data, objective evaluations can be performed on fingerprint readers. Additionally, the data collected could be utilized to learn fingerprint distortion models, fingerprint reader interoperability calibration models, and latent fingerprint distortion models. Finally, the universal fingerprint targets will be used to assess the spoofing vulnerability of various fingerprint recognition systems (such as smartphones).

Acknowledgment

This research was supported by grant no. 70NANB15H280 from the NIST Measurement Science program. The authors would like to thank Brian Wright, Michigan State University, for his help in 3D printing of molds. We would also like to thank Edward Drown, Michigan State University, for his help mixing castings materials for the universal fingerprint targets.

References

[1] D. Maltoni, D. Maio, A. K. Jain, and S. Prabhakar, *Handbook of Fingerprint Recognition*. Springer, 2nd ed., 2009.

[2] C. I. Watson, G. Fiumara, E. Tabassi, S. Cheng, P. Flanagan, and W. Salamon, "Fingerprint vendor technology evaluation, nist interagency/internal report 8034: 2015," available at https://dx.doi.org/10.6028/NIST.IR.8034.

[3] S. S. Arora, K. Cao, A. K. Jain, and N. G. Paulter, "Design and fabrication of 3d fingerprint targets," *IEEE Transactions on Information Forensics and Security*, vol. 11, pp. 2284–2297, Oct. 2016.
[4] S. S. Arora, A. K. Jain, and N. G. Paulter, "3d whole hand targets: Evaluating slap and contactless fingerprint readers," in *2016 International Conference of the Biometrics Special Interest Group (BIOSIG)*, pp. 1–8, Sept 2016.
[5] S. S. Arora, A. K. Jain, and N. G. Paulter, "Gold fingers: 3d targets for evaluating capacitive readers," *IEEE Transactions on Information Forensics and Security*, pp. 1–1, Apr. 2017.
[6] Smooth-On, *Silicone Silc Pig Technical Data Sheet*. available at https://www.smooth-on.com/tb/files/Silc_Pig_Pigments.pdf.
[7] Dow Corning, *Sylgard PDMS 184 Data Sheet*. http://www.dowcorning.com/DataFiles/090276fe80190b08.pdf.
[8] Silicone Solutions, *SS-27S Technical Data Sheet*. available at http://siliconesolutions.com/media/pdf/SS-27STDS.pdf.
[9] Smooth-On, *Silicone Thinner Technical Data Sheet*. available at https://www.smooth-on.com/tb/files/Silicone_Thinner.pdf.
[10] C. Edwards and R. Marks, "Evaluation of biomechanical properties of human skin," *Clinics in Dermatology*, vol. 13, no. 4, pp. 375 – 380, 1995. Bioengineering of the Skin.
[11] V. Falanga and B. Bucalo, "Use of a durometer to assess skin hardness," *Journal of the American Academy of Dermatology*, vol. 29, no. 1, pp. 47 – 51, 1993.
[12] T. Faes, H. Van der Meij, J. De Munck, and R. Heethaar, "The electric resistivity of human tissues (100 hz-10 mhz): a meta-analysis of review studies," *Physiological measurement*, vol. 20, no. 4, p. R1, 1999.
[13] Stratsys, *Digital Material Technical DataSheet*. available at http://global72.stratasys.com/~/media/Main/Files/Material_Spec_Sheets/MSS_PJ_PJMaterialsDataSheet.pdf#_ga=2.193296616.455247396.1494258560-1158297905.1493673102.
[14] "Resistivity of gold." https://hypertextbook.com/facts/2004/JennelleBaptiste.shtml.
[15] "Applied Image Inc." https://www.appliedimage.com/.
[16] "NIST fingerprint testing and standards." http://slideplayer.com/slide/3358135/.
[17] "Medical Expo, THE ONLINE MEDICAL DEVICE EXHIBITION." http://www.medicalexpo.com/medical-manufacturer/test-phantom-2563.html. Accessed: 2017-2-07.
[18] "IAFIS FAQs." https://www.fbibiospecs.cjis.gov/Certifications/FAQ.
[19] R. Black, *Managing the Testing Process: Practical Tools and Techniques for Managing Hardware and Software Testing*. Wiley Publishing, 3rd ed., 2009.
[20] "Pacific Northwest X-Ray Inc." http://www.pnwx.com/Accessories/Phantoms/Radiology/?Sr=Go&gclid=CPesworu59ECFcS6wAodoZ4MTQ. Accessed: 2017-2-07.
[21] S. Orandi, F. Byers, S. Harvey, M. Garris, S. Wood, J. Libert, and J. Wu, "Standard calibration target for contactless fingerprint scanners, NIST patent," 2016-05-24.
[22] A. Ross and A. Jain, *Biometric Sensor Interoperability: A Case Study in Fingerprints*, pp. 134–145. Springer, 2004.
[23] A. Ross and R. Nadgir, "A thin-plate spline calibration model for fingerprint sensor interoperability," *IEEE Trans. on Knowl. and Data Eng.*, vol. 20, pp. 1097–1110, Aug. 2008.
[24] S. Moore, "Latest tests of biometrics systems shows wide range of abilities," *IEEE Spectrum Online*, 2004. available at http://spectrum.ieee.org/computing/embedded-systems/latest-tests-of-biometrics-systems-shows-wide-range-of-abilities.
[25] A. K. Jain, S. Prabhakar, and A. Ross, "Fingerprint matching: Data acquisition and performance evaluation," Tech. Rep. MSUTR99-14, Department of Computer Science, Michigan State University, East Lansing, Michigan, March 1999.
[26] S. K. Modi, S. J. Elliott, and H. Kim, "Statistical analysis of fingerprint sensor interoperability performance," in *Proceedings of the 3rd IEEE International Conference on Biometrics: Theory, Applications and Systems*, pp. 294–299, 2009.
[27] "Unique Identification Authority of India, dashboard summary." https://portal.uidai.gov.in/uidwebportal/dashboard.do.
[28] "UIDAI biometric device specifications (authentication)." http://www.stqc.gov.in/sites/upload_files/stqc/files/UIDAI-Biometric-Device-Specifications-Authentication-14-05-2012_0.pdf.
[29] "Hand anthropometry." http://usability.gtri.gatech.edu/eou_info/hand_anthro.php.
[30] Stratsys, *Stratasys Connex Printer Machine Specifications*. http://www.stratasys.com/~/media/Main/Files/Machine_Spec_Sheets/PSS_PJ_Connex3.ashx.
[31] "Speedmixer." http://speedmixer.com/.
[32] Smooth-On, *Silicone Ease Release 200 Technical Data Sheet*. available at https://www.smooth-on.com/tb/files/er200.pdf.
[33] "Perkin elmer lambda 900 uv-vis spectrometer." http://www.perkinelmer.com/category/uv-vis-spectroscopy-uv.
[34] C. C. Cooksey, B. K. Tsai, and D. W. Allen, "Spectral reflectance variability of skin and attributing factors," in *Proc. SPIE*, vol. 9461, p. 94611M, 2015.
[35] Keyence, *Keyence Optical Digital Microscope VHX-600*. http://www1.keyence.eu/products/microscope/microscope/vhx6002/vhx6002specifications1.php.
[36] "Gamry electro-chemical spectrometer." https://www.gamry.com/potentiostats/.
[37] AEP Technology, *NANOMAP-500LS*. http://www.aeptechnology.com/pdfs/NanoMap-500LS.pdf.
[38] "NIST special database 4." https://www.nist.gov/srd/nist-special-database-4.
[39] "FVC2002." http://bias.csr.unibo.it/fvc2002/. 2002.
[40] "FVC2004." http://bias.csr.unibo.it/fvc2004/. 2004.
[41] "Fingerprint matching software." https://www.innovatrics.com/idkit-fingerprint-sdk/.
[42] L. Hong, Y. Wan, and A. Jain, "Fingerprint image enhancement: Algorithm and performance evaluation," *IEEE Trans. Pattern Anal. Mach. Intell.*, vol. 20, pp. 777–789, Aug. 1998.

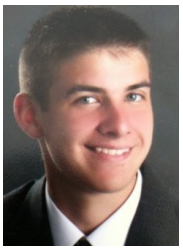

Joshua J. Engelsma graduated magna cum laude with a B.S. degree in computer science from Grand Valley State University, Allendale, Michigan, in 2016. He is currently working towards a PhD degree in the Department of Computer Science and Engineering at Michigan State University, East Lansing, Michigan. His research interests include pattern recognition, computer vision, and image processing with applications in biometrics.

Sunpreet S. Arora received the B.Tech. (Hons.) degree in Computer Science from the Indraprastha Institute of Information Technology, Delhi (IIIT-D) in 2012, and the Ph.D. degree in Computer Science and Engineering from Michigan State University, in 2016. He is currently a Senior Biometrics Researcher at Visa Inc., Foster City, CA. His research interests include biometrics, pattern recognition and image processing. He received the best paper award at the 15th IEEE BIOSIG, 2016, and the best poster award at the IEEE BTAS, 2012.

Anil K. Jain is a University distinguished professor in the Department of Computer Science and Engineering at Michigan State University. His research interests include pattern recognition and biometric authentication. He served as the editor-in-chief of the IEEE Transactions on Pattern Analysis and Machine Intelligence. He is a member of the United States National Academy of Engineering and a Foreign Fellow of the Indian National Academy of Engineering.

Nicholas G. Paulter Jr. is the Group Leader for the Security Technologies Group at NIST in Gaithersburg, MD. He develops and oversees metrology programs related to concealed weapon and contraband imaging and detection, biometrics for identification, and body armor characterization. He has authored or co-authored over 100 peer-reviewed technical articles and provided numerous presentations at a variety of technical conferences. He is a 2008-2009 Commerce Science and Technology Fellow and a 2010 IEEE Fellow